Vol. 516: 71–83, 2014
doi: 10.3354/meps10833

MARINE ECOLOGY PROGRESS SERIES
Mar Ecol Prog Ser

Published December 3

Optical characterization and distribution of chromophoric dissolved organic matter (CDOM) in soil porewater from a salt marsh ecosystem

Catherine D. Clark[1,2,*], Paige Aiona[1], Jason K. Keller[1], Warren J. De Bruyn[1]

[1]School of Earth and Environmental Sciences, Schmid College of Science and Technology, Chapman University, 1 University Drive, Orange, CA 92866, USA

[2]*Present address:* Department of Chemistry, College of Science and Engineering, Western Washington University, Bellingham, WA 98225, USA

ABSTRACT: To characterize chromophoric dissolved organic matter (CDOM) in marsh porewaters and its contribution as a carbon source, optical properties (absorbance, fluorescence indices, 3-dimensional excitation-emission matrices [EEMs]) of soil porewater and surface water were measured in a southern Californian salt marsh. Absorption coefficients and fluorescence intensities were higher in porewater than in overlying surface waters, consistent with higher CDOM concentration at depth. Humic-type peaks A and C were observed in EEMs in all samples, and peak M was observed in surface waters and shallow porewater to −5 cm depth. Fluorescence: absorbance (flu:abs) ratios and spectral slopes (S) decreased across the surface interface, and emission peak maxima were red-shifted — changes that are consistent with increasing molecular weight (MW) and aromaticity in soil porewater due to humification, and lower-MW, less aromatic material in oxic surface waters from oxidative photochemical and biological processing. At lower depths, bands were observed where intensity, flu:abs ratios and S increased; absorption coefficients decreased; emission maxima for humic-type peaks were blue-shifted; and tryptophan-type protein peaks were observed. These changes are consistent with lower-MW and less aromatic material from enhanced microbial activity. Variations in iron concentrations and sulfate depletion with depth were consistent with these bands having different dominant anaerobic microbial metabolic pathways. Overall, optical property trends suggest that soil porewater is a reservoir of CDOM in the salt marsh, with organic material from terrestrial watershed inputs and *in situ* production from marsh vegetation stored and processed in sediments.

KEY WORDS: Salt marsh · Dissolved organic matter · CDOM · Fluorescence · Intertidal sediments · Optical properties

INTRODUCTION

Salt marshes are tidally forced wetlands that act as key transformers of carbon as it moves between adjacent terrestrial and marine ecosystems (Tobias & Neubauer 2009). They sequester significant amounts of organic carbon in their soils (Chmura et al. 2003) because of an imbalance between inputs from sedimentation and production by plants and algae and outputs through microbial decomposition and export. Carbon is exported and exchanged as dissolved inorganic carbon, particulate organic matter and dissolved organic matter (DOM) (Tobias & Neubauer 2009). While the magnitude and composition of exported carbon varies based on hydrology, productivity and geomorphology, most North American Atlantic and Gulf Coast marshes are significant DOM exporters (Moran & Hodson 1994, Rochelle-Newall & Fisher 2002, McLusky & Elliot 2004, Gallegos et al. 2005, Gardner et al. 2005).

*Corresponding author: catherine.clark@wwu.edu

Marsh-derived DOM plays an important role in adjacent marine ecosystems in microbial food webs, regulation of photochemistry and light availability and mediation of nutrient and pollutant availability (Tzortziou et al. 2011, references therein).

One approach to examine carbon sources and transformations in wetlands is the optical properties of the light-absorbing fraction of DOM (chromophoric DOM [CDOM]; Vodacek et al. 1997, Miller 1998). CDOM affects aquatic chemistry and carbon biogeochemical cycling through sunlight-initiated photochemical processes (Moran & Zepp 1997). Optical characterization methods (e.g. spectral slopes, fluorescence:absorbance [flu:abs] ratios, 3-dimensional excitation-emission matrix [EEM] fluorescence spectra) have been used to evaluate the sources, distribution and fate of CDOM (Coble 1996, Boyd & Osburn 2004). In particular, CDOM fluorescence has proved a sensitive tool for studying DOM sources and transport in estuarine and coastal waters (Rochelle-Newall & Fisher 2002, Stedmon et al. 2003, Chen & Gardner 2004). The few published studies on optical properties of salt marsh-derived CDOM have primarily focused on the USA eastern Atlantic and Gulf Coasts, and Europe (Moran et al. 2000, Gardner et al. 2005, Tzortziou et al. 2007, Otero et al. 2007), where coastal waters are dominated by freshwater riverine inputs. Production of DOM from detritus of vascular salt marsh plant species in these ecosystems has been demonstrated (Moran & Hodson 1989, 1994, Vahatalo & Wetzel 2008, Wang et al. 2007).

Our previous work in Pacific Ocean systems on the west coast of the United States indicated that salt marshes were the primary source of CDOM to coastal waters in the absence of rain events and associated riverine inputs in regions with a semi-arid Mediterranean-type climate (Clark et al. 2008). The exported CDOM did not appear to be freshly produced material from marsh plants based on plant leachate studies, and we hypothesized that soils were the major carbon reservoir and primary source of exported DOM (Clark et al. 2008). To characterize salt marsh soil CDOM and assess the contribution of soil porewater as a carbon reservoir, in this study we measured optical properties of CDOM in surface water and soil porewater as a function of depth. Results are compared to measurements in adjacent coastal receiving waters and salt marsh porewater in other climate regions. These are the first results reported for salt marsh porewater in a Pacific Ocean ecosystem.

MATERIALS AND METHODS

Site description

The site is a ~0.25 km^2 salt marsh discharging into the Santa Ana River (SAR) outlet in Huntington Beach, Orange County, southern California (site map in Clark et al. 2008). The US Army Corps of Engineers acquired this land from an oil company in early 1990. Restoration was completed in 1992 as mitigation for the adjacent river channelization for flood control. Channels were excavated for restoration with native vegetation (pickleweed *Salicornia virginica*, saltbush *Atriplex lentiformis*, sea-fig *Carpobrotus chilensis*, saltwort *Batis maritima*, alkali health *Frankenia grandiflora*). The river only flows during and immediately after significant rain events in the upper watershed, otherwise, the outlet is tidally flushed with no freshwater flow. Tide gates between the SAR and marsh provide tidal influence with inflowing ocean water on a flood tide and outflowing water at ebb. Surface water salinities range from 30 to 33 (Clark et al. 2008). To examine marsh output, samples were taken on the bank of the main channel discharging through tide gate Stn W5 (33° 38.111′ N, 117° 57.298′ W) into the adjacent SAR (site description and figure in Clark et al. 2008). Locations were 10 m from Stn W5 at 1 and 2 m from the main channel (sites A and B, respectively). Water samples were collected from above (heights expressed as positive-value depths) and below (depths expressed as negative-value depths) the water-ediment surface interface.

Sampling

Soil porewater was sampled in winter 2010 from 12 to 26 February ('winter') using porewater equilibrators (peepers, Hesslein 1976) constructed from plexiglass (12 × 75 cm) with ~30 ml sampling chambers every 3 cm. Sampling chambers were filled with distilled water and covered with a 0.2 µm Versapor membrane (Pall) held in place with plexiglass covers; the membranes act as filters during sample collection. Assembled peepers were submerged in degassed distilled water to pre-equilibrate for 2 wk before deployment. A guide was driven into exposed marsh soil to a depth of approximately −30 cm during low tide, and peepers were inserted into the resulting hole. Peepers were situated so the first sampling chamber below the soil surface had an average depth of −1.5 cm, and the first chamber above the soil was

at an average height of 1.5 cm. Site A sampled porewater to a depth of −31.5 cm, whereas site B sampled to −28.5 cm. Peepers were deployed for 2 wk (12–26 February) to equilibrate with surrounding porewater. Over this period, tidal heights ranged from 0.4 to 0.8 m. During the sampling period, surface water was collected at both sites 4.5 cm above ground level, consistent with inundation at high tide. In February, 2 rainfall events occurred: a 7 cm rainfall on 6 February (6 d before deployment) and a 0.3 cm rainfall during deployment on 24 February (SAR, https://media.ocgov.com/gov/pw/watersheds/rainrecords). Upon collection, water was removed from each sampling chamber using plastic Luer lock syringes and injected into evacuated serum bottles in the field. Samples were returned to the laboratory and stored in the dark at 4°C until optical analyses were performed over the next 2 wk. Winter samples were not refiltered in the laboratory. A single sample (−28.5 cm at site B) was excluded from analysis, as it was contaminated during sampling.

To assess seasonal differences, we redeployed at site A from 6 to 20 July 2012 ('Summer'). Over the 2 wk equilibration period, tidal heights ranged from 0.05 to 1.0 m. There was no rain in June pre-deployment, and a single 0.5 cm rain event occurred on 13 July (SAR, https://media.ocgov.com/gov/pw/watersheds/rainrecords). Water was collected 7.5 cm above the soil, consistent with inundation at high tide. Samples were collected as before (i.e. filtered *in situ* through the 0.2 µm peeper membrane) but were stored in syringes equipped with 2-way stopcocks for transport and refiltered in the laboratory (0.2 µm polyvinylidene difluoride filters) in an anaerobic glove box (<2% H_2 headspace with balance of N_2; Coy Laboratory Products) to minimize oxygen exposure prior to the iron and sulfur analyses.

Optical characterization

Absorbance spectra were measured with a diode-array UV-visible spectrometer (Agilent 8453) from 200 to 700 nm in a quartz cell (path length = 10 cm) with a deionized water blank. Instrument specifications give a spectral resolution of <2 nm and stray light of <0.03%. Absorbance was transformed to the Napierian absorption coefficient (m^{-1}) by multiplying the measured absorbance at 300 and 350 nm by 2.303 and dividing by path length (in m) (Hu et al. 2002); 300 nm is a wavelength commonly used for CDOM intercomparisons (Miller 1998). Spectral slopes (S) were calculated from Eq. (1) with a first-order linear regression for 3 regions**:** 300 to 400 nm (S_1) for comparison to our previous work (Clark et al. 2008, 2009, 2010), and 275 to 295 (S_2) and 350 to 400 nm (S_3) as recommended by Helms et al. (2008):

$$-S = (\ln Abs/A_0)/(\lambda - \lambda_0) \quad (1)$$

where Abs is absorbance at wavelength λ, and A_0 is absorbance at reference wavelength λ_0 (Green & Blough 1994, Moran et al. 2000). For S_2 and S_3, R^2 is >0.999, with $p < 0.0001$. Helms et al. (2008) found <1% difference for small spectral windows (25 to 50 nm for S_2 and S_3) between S calculated from a non-linear exponential fit to Eq. (1) vs. the linear regression to log-transformed values used here (N = 48). The 100 nm range for S_1 in this study appears to be well fit by the linear regression method ($R^2 > 0.985$, $p < 0.0001$). Slope ratio (S_R) is calculated as S_2/S_3 (Helms et al. 2008).

Three-dimensional EEM fluorescence spectra were obtained with a scanning fluorometer (Quantamaster, PTI) by ranging excitation wavelengths from 260 to 430 nm in 5 nm increments and emission from 260 to 650 nm in 5 nm increments. A water EEM (Whatman Nanopure ion exchanger) was generated daily to subtract out the water Raman peak and Rayleigh scattering. Spectra were corrected for instrumental response using the manufacturer's correction file. Percent error on 3 duplicate absorbance and fluorescence scans was <0.5%. Fluorescence intensities (photons s^{-1}) were converted to quinine sulfate units (QSU; 1 QSU = 1 ppb quinine sulfate in 0.05 M H_2SO_4) with a calibration curve (Mopper & Schultz 1993). Samples were diluted prior to fluorescence measurements to minimize inner filter effects as described in Burdige et al. (2004).

Three fluorescence indices were calculated following methods summarized in Huguet et al. (2010), specifically (1) $f450/f500$, the ratio of fluorescence intensities at 450 and 500 nm at an excitation of 370 nm; (2) HIX, the ratio of the areas between 435 and 480 nm to 399 and 345 nm at an excitation of 254 nm (in our study, we used 260 nm, as this was the lowest wavelength we scanned); and (3) BIX, the ratio of the intensities at 380 and 430 nm at an excitation of 310 nm.

Iron and sulfur analyses

To explore potential changes in the microbial carbon mineralization pathways, we measured iron and sulfur in summer. Dissolved Fe(II) was measured on porewater samples immediately after filtering in the

anaerobic chamber. Then, 1.0 ml of porewater was added to a buffered ferrozine solution (0.1% ferrozine in HEPES buffer, pH = 7.0), and absorbance at 562 nm was immediately measured (Lovley & Phillips 1986). Subsamples of filtered porewater were frozen (–4°C) until analysis for dissolved sulfate and chloride on a Dionex ion chromatography system with an anion self-regenerating suppressor. Thawed samples were diluted using Nanopure water and analyzed isocratically using an AG11-HC guard column, an AS11-HC column and a 25 mM NaOH eluent. Based on measured sulfate and chloride values, sulfate depletion was calculated as:

$$SO_4 \text{ depletion} = [(Cl^-_{PW}) \times (R_{SW})^{-1}] - SO_4^{2-}{}_{PW} \quad (2)$$

where (Cl^-_{PW}) and $(SO_4^{2-}{}_{PW})$ are Cl^- and SO_4^{2-} porewater concentrations (in mM) from ion chromatography, respectively, and R_{SW} is the constant molar ratio of Cl^- to SO_4^{2-} in surface seawater (19.33; Bianchi 2007). Positive SO_4 depletion values represent a net depletion of SO_4^{2-} compared to the value predicted by the seawater Cl^-:SO_4^{2-} ratio, presumably from sulfate reduction by the microbial community (Keller et al. 2009).

RESULTS

There was good agreement between absorption coefficients measured at 300 and 350 nm (a300 and a350) at sites A and B in winter (Table 1). For example, a300 at site A increased from 2 m^{-1} at the surface to 14 m^{-1} at 13.5 cm depth, while at site B, an increase in a300 from 1 m^{-1} at the surface to 13 m^{-1} at 13.5 cm depth was observed. Deeper in the porewater column, a300 values decreased before increasing back to 16 m^{-1} for site A and 11 m^{-1} for site B at –19.5 cm depth. At site A, a300 then decreased to 11 m^{-1} at –28.5 cm depth and increased back to 15 m^{-1} at –31.5 cm. At site B, a300 increased from 11 m^{-1} at –19.5 cm depth to 13 m^{-1} at –25.5 cm. Similar trends were observed in summer, with a300 increasing from 3 m^{-1} in surface waters to 13 m^{-1} just below the surface (–1.5 cm depth) and to a maximum of 54 m^{-1} at –28.5 cm depth. Increases in absorption coefficient were observed at depths of –16.5, –19.5 and –28.5 cm (Table 1). In both seasons, a300 for surface water was within range of prior studies at this marsh (Clark et al. 2008).

Fluorescence trends differed from those observed for absorption. In winter, intensities initially decreased below the surface and then increased in bands at –7.5, –16.5 and –28.5 cm depth (Table 1). In summer, intensities were lower in surface water and increased across the soil interface into shallow porewater (Table 1), then decreased at –4.5 to –7.5 cm depth followed by an increase to a maximum at –25.5 cm and a decrease to –31.5 cm. In summer, fluorescence intensities were lower in surface water (factor of 10) and shallower porewater (factor of 1.5 to 2) but comparable below –13.5 cm depth.

S values were calculated over 3 spectral ranges (S_1, 300 to 400 nm; S_2, 275 to 295 nm; S_3, 350 to 400 nm) which all showed the same general trends. Note that slopes are negative, but absolute values are reported: increasing *S* corresponds to a steeper slope (more negative number) and a larger reported absolute value. In winter, S_1 (mean ± SD) was 0.012 ± 0.002 nm^{-1} in surface water to <0.002 nm^{-1} at –7 cm depth (Table 1). After an initial decrease in *S* over the first few centimeters, 2 maxima occurred at depths of –15 to –20 cm and –25 to –30 cm, concurrent with minima and maxima in absorbance and fluorescence (Table 1). Winter S_R varied from 0.56 to 2.8, averaging 1.17 ± 0.53 (mean ±1 SD) for all samples at both sites. Surface water and transitional samples (from 4.5 cm above to 4.5 cm below the surface) averaged 0.97 ± 0.15, whereas samples below –4.5 cm were higher, 1.26 ± 0.61. In summer, S_1 ranged from 0.011 ± 0.008 nm^{-1} in surface water to 0.007 nm^{-1} at –28.5 cm depth (Table 1). In contrast to winter, S_1 increased from 0.015 to 0.018 nm^{-1} in porewater at –1.5 to –13.5 cm depth, followed by decreases to <0.01 nm^{-1} at –16.5 and –28.5 cm depth. Summer S_R values were similar to winter, varying from 0.5 to 2.0 and averaging 1.00 ± 0.87 for surface waters and 1.28 ± 0.87 for porewater.

Three-dimensional EEMs have been shown to distinguish between CDOM sources in natural waters (Coble 1996, de Souza Sierra et al. 1997, McKnight et al. 2001). Peak locations and classifications used here follow Coble (1996), with 5 main fluorescent peaks with distinct excitation and emission wavelength regions: (1) peak B, tyrosine protein-like (maximum excitation wavelength:maximum emission wavelength 275/310 in nm); (2) peak T, tryptophan protein-like (275/340); (3) peak A, humic-like (260/380–460); (4) peak M, microbial humic-like 312/380–420); and (5) peak C, terrestrial humic-like (350/420–480). Parallel factor analysis (PARAFAC), which can identify fluorescent components beyond the Coble model, was not used in this study because of the limited size of the database (PARAFAC models are based on hundreds to thousands of sample EEMs; Stedmon et al. 2003, Stedmon & Markager 2005, Murphy et al. 2008).

Table 1. Optical characteristics of salt marsh chromophoric dissolved organic matter (absorption coefficients at 300 and 350 nm [a300 and a350; m^{-1}], spectral slopes [S_1, 300 to 400 nm; S_2, 275 to 295 nm; S_3, 350 to 450 nm], spectral slope ratio [S_R; S_2/S_3], fluorescence intensities [Flu in quinine sulfate units, QSU; excitation = 350 nm, emission = 450 nm] and peak excitation/emission (ex/em) maxima [nm]) for humic excitation-emission matrix peaks A and C for samples collected in winter 2010 at sites A and B and in summer 2011 at site A. –: not determined

Depth (cm)	a300	a350	Flu	S_1	S_2	S_3	S_R	Peak A (ex/em)	Peak C (ex/em)
Winter									
Site A									
4.5	2.0	1.1	124	0.012	0.011	0.011	1.00	260/445	345/435
1.5	1.8	1.0	112	0.013	0.011	0.014	0.79	260/445	345/430
–4.5	3.4	2.5	97	0.0057	0.0055	0.0062	0.89	260/445	345/430
–7.5	7.8	7.3	112	0.001	0.0019	0.001	1.90	260/465	345/445
–10.5	14.4	13.6	95	0.0012	0.0012	0.0016	0.75	260/465	345/440
–13.5	13.8	13.2	92	0.0012	0.0009	0.0016	0.56	260/465	345/445
–16.5	8.9	7.5	133	0.0032	0.0035	0.0032	1.09	260/460	345/445
–19.5	16.4	15.4	91	0.0016	0.0011	0.0022	0.50	260/465	345/445
–22.5	11.6	10.4	121	0.002	0.0027	0.0021	1.29	260/465	345/445
–25.5	12.3	11.6	116	0.0011	0.0017	0.0012	1.42	260/465	345/440
–28.5	10.7	8.2	199	0.0064	0.0046	0.008	0.58	260/445	345/440
–31.5	15.1	14.5	139	0.0007	0.0014	0.0009	1.56	260/460	345/440
Site B									
4.5	1.1	0.5	90	0.015	0.013	0.015	0.87	260/440	345/435
1.5	1.3	0.8	96	0.011	0.011	0.010	1.10	260/435	345/430
–1.5	6.3	5.8	86	0.0017	0.0023	0.0019	1.21	260/465	345/445
–4.5	10.6	10.0	78	0.0011	0.0013	0.0014	0.92	260/465	345/445
–7.5	13.1	12.8	166	0.0005	0.0009	0.0007	1.28	260/445	345/440
–10.5	12.9	12.4	84	0.001	0.0009	0.0014	0.64	260/465	345/445
–13.5	13.3	12.9	86	0.0007	0.001	0.0008	1.25	260/465	345/435
–16.5	4.9	3.4	192	0.007	0.0078	0.0071	1.10	260/450	345/440
–19.5	11.1	10.0	149	0.0017	0.003	0.0016	1.89	260/465	345/440
–22.5	11.7	10.6	166	0.0019	0.0032	0.002	1.60	260/465	345/440
–25.5	13.4	12.8	161	0.0011	0.0025	0.0009	2.8	260/465	345/440
Summer									
7.5	3.3	1.78	8	0.011	0.002	0.004	0.50	260/440	340/435
4.5	3.8	2.5	7	0.007	0.001	0.002	0.50	260/445	340/425
1.5	8.95	6.43	22	0.006	0.004	0.002	2.00	260/450	340/425
–1.5	13.2	5.63	71	0.018	0.015	0.019	0.79	260/445	340/425
–4.5	6.55	3.15	44	0.015	0.009	0.010	0.90	260/425	340/420
–7.5	4.07	1.33	46	–	0.008	–	–	260/435	340/425
–10.5	6.4	3.05	66	0.015	0.009	0.010	0.90	260/435	340/425
–13.5	8.7	1.58	74	0.017	0.017	0.012	1.42	260/445	340/425
–16.5	37.7	32.6	82	0.001	0.004	0.001	4.00	260/450	340/430
–19.5	41.6	24.1	99	0.011	0.006	0.013	0.46	260/440	340/435
–22.5	35.6	19.6	131	0.011	0.010	0.007	1.43	260/450	340/430
–25.5	27.9	13.2	150	0.016	0.014	0.016	0.88	260/445	340/435
–28.5	53.7	38.4	124	0.007	0.006	0.006	1.00	260/450	340/430
–31.5	18.8	8.7	117	0.010	0.012	0.008	1.50	260/450	340/430

Peaks at sites A and B showed similar trends with depth. Representative EEMs are shown in Fig. 1 for site A in winter. Protein-like peaks were not observed in surface water and most porewater samples but occurred at –16.5 and –28.5 cm, coincident with decreases in a300 and increases in fluorescence (Table 1). M peaks, similar in intensity to A peaks, were observed in surface water and shallow porewater samples to –4.5 cm depth (Fig. 1). Peaks A and C were identified in surface and porewater from all depths, with intensities increasing with depth to –7 cm by 120 QSU as maximum emission intensities were red-shifted by 25 and 15 nm for A and C, respectively. Some oscillations were seen from –7 to –32 cm depth, where intensities decreased and wavelengths were blue-shifted. Representative EEMs vs. depth are shown in Fig. 2 for summer. Peaks A and C were again identified in surface and

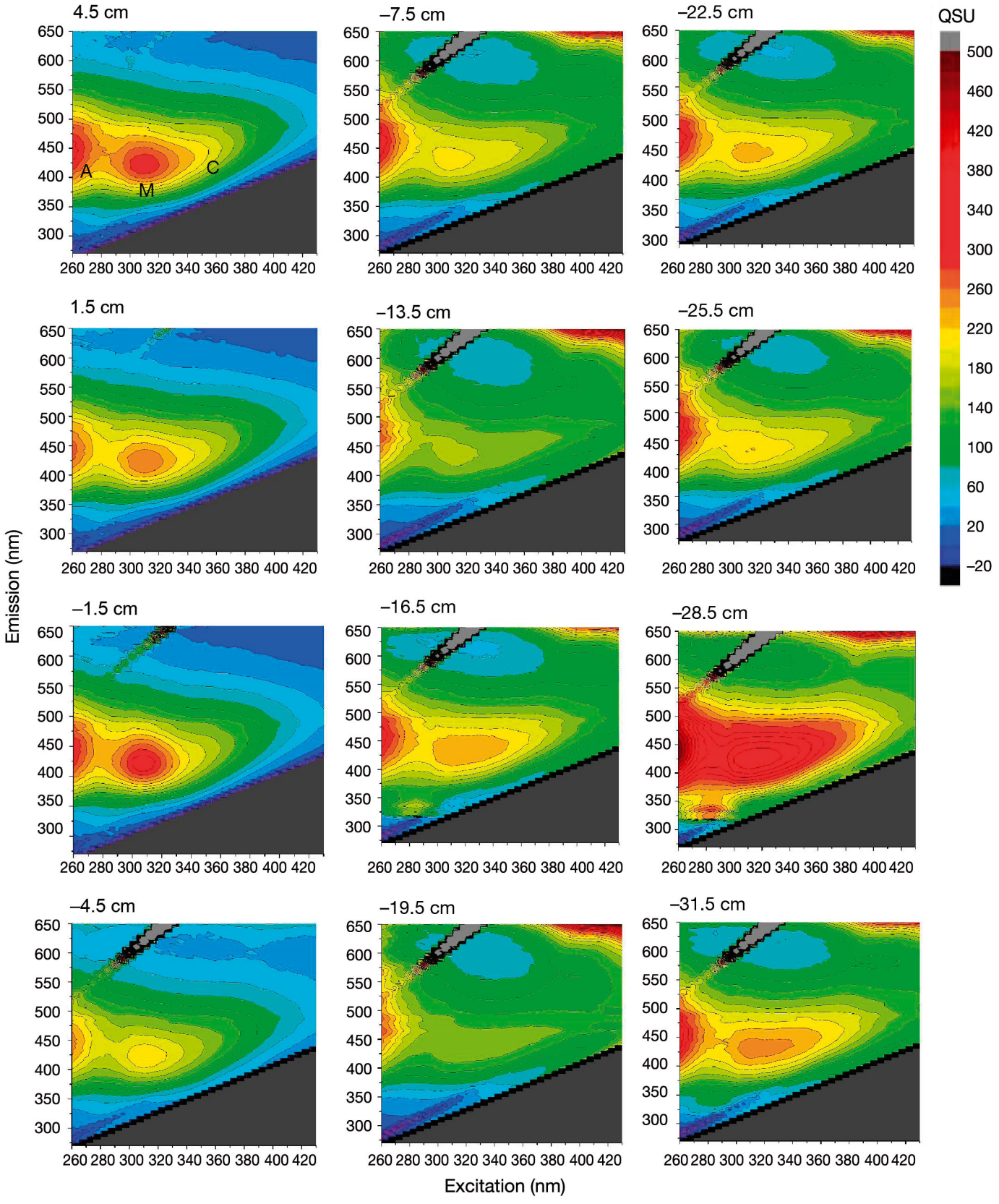

Fig. 1. Contour plots of 3-dimensional excitation-emission matrices as a function of depth (cm) for site A in winter; *x*-axis: $\lambda_{excitation}$ from 260 to 430 nm in increments of 20 nm; *y*-axis: $\lambda_{emission}$ from 260 to 650 nm in increments of 50 nm. Contour lines represent intensities from 0 (blue) to 500 (dark red) quinine sulfate units (QSU) in increments of 20. Humic peaks M, A and C are labeled for the surface water sample (4.5 cm)

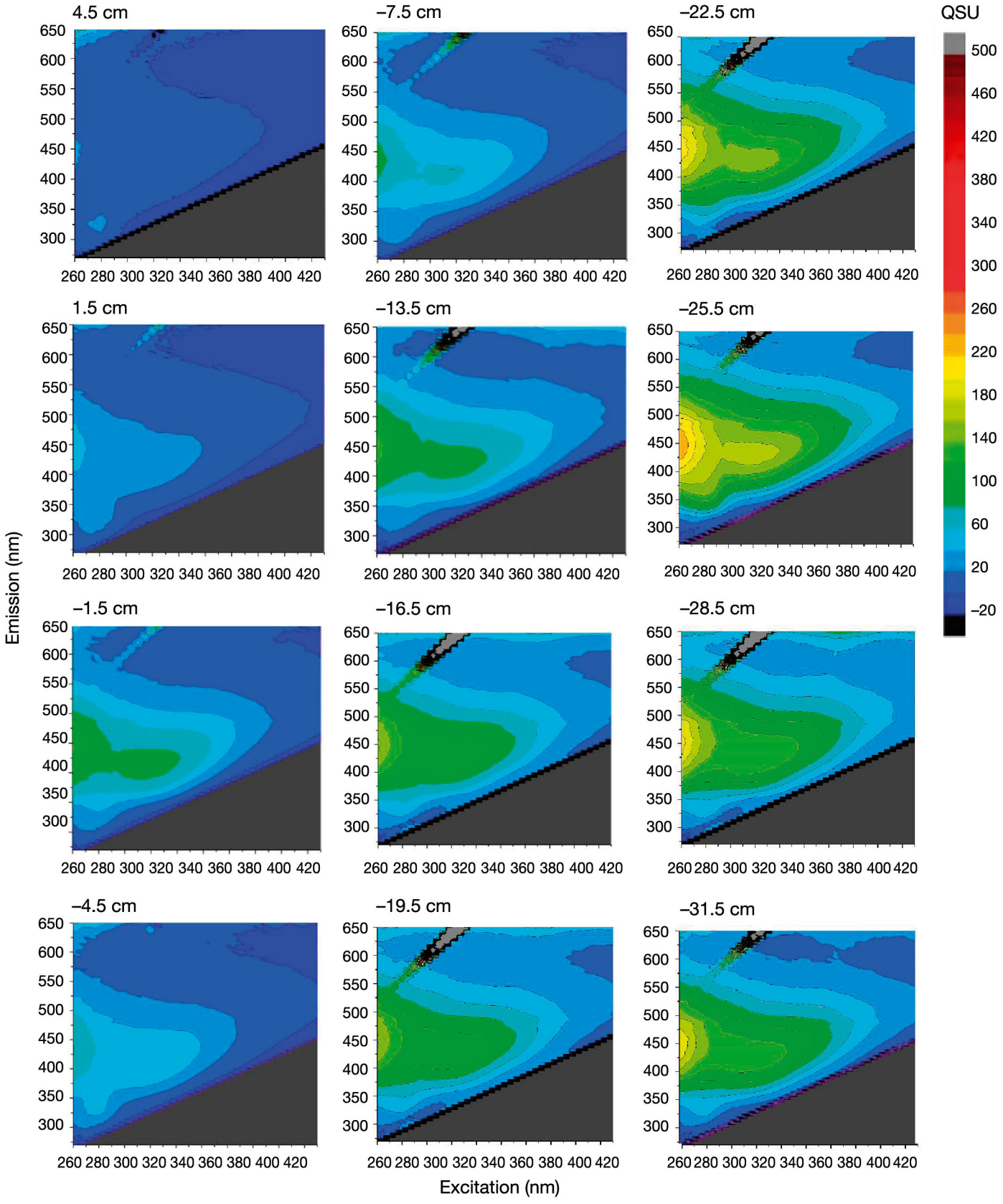

Fig. 2. Contour plots of 3-dimensional excitation-emission matrices as a function of depth (cm) for site A in summer; *x*-axis: $\lambda_{excitation}$ from 260 to 430 nm in increments of 20 nm; *y*-axis: $\lambda_{emission}$ from 260 to 650 nm in increments of 50 nm. Contour lines represent intensities from 0 (blue) to 500 (dark red) quinine sulfate units (QSU) in increments of 20

porewater from all depths but at lower intensities. The most intense protein-like peaks were at −25.5 cm, where a300 decreased and fluorescence increased (Table 1). In contrast to winter, no M peaks were observed in surface or shallow porewaters. Higher peak A and C intensities were observed from −22.5 through −28.5 cm with intense protein peaks. Another feature with excitation at 400 to 420 nm and emission at 630 to 650 nm was observed in pore water samples below −7.5 cm, most notably at depths of −16.5 cm and −28.5 cm and at higher intensities in winter vs. summer. Based on the optical characteristics, we attribute this feature to chlorophyll or pheophytin, a degradation product of chlorophyll (French et al. 1956).

The $f450/f500$ nm index averaged 1.3 and 1.8 for surface water samples in winter and summer, respectively. Porewater samples in winter averaged 1.2 across all depths, except for slight increases to 1.3 at depths of −16.5 and −28.5 cm. In summer, values in the shallower porewaters to a depth of −10.5 cm averaged 1.5, and the deeper porewaters averaged 1.3. The calculated average values had a standard deviation of ±0.1. HIX values in summer ranged from 1.8 ± 0.3 for the surface waters to 4.5 ± 0.2 for the porewater. In winter, HIX averaged 7 ± 0.8 in the surface waters and 10 ± 1 in most of the porewater samples. Decreased values (5 ± 2) were observed at depths of −7.5, −16.5 and −28.5 cm. In winter, BIX values averaged 0.66 ± 0.6 in both surface waters and porewaters. In summer, BIX values averaged 0.73 ± 0.4 in the surface and deeper porewaters and 0.86 ± 0.3 in the shallower porewaters to a depth of −10.5 cm.

To assess potential differences in porewater microbial processing, we measured dissolved iron and sulfur in the summer study. Fe(II) concentrations increased from near zero in surface and shallow porewater to 286 µM at −16.5 cm depth followed by a decrease to 5 µM at −28.5 cm (Fig. 3). SO_4 depletion was fairly constant, around 0 mM, in surface waters and porewater to −4.5 cm depth, increasing to 8 mM at −28.5 cm depth and decreasing at −31.5 cm. The rate of increase in SO_4 depletion with depth decreased at −16.5 cm, where a spike in Fe(II) concentration occurred. The reverse was observed at −28.5 cm, where a peak in SO_4 depletion corresponded to decreasing Fe(II) concentration. These results are consistent with sulfate reduction as the dominant anaerobic microbial process, except for porewater at −16.5 cm depth, where higher Fe(II) levels suggest that anaerobic microbial carbon mineralization may be occurring via iron rather than sulfate reduction (Megonigal et al. 2004). While rates of sulfate and iron reduction are not available for this site, variations in iron and sulfate levels with depth have been observed in marshes near this region (Berner 1964, Leslie et al. 1990, Elrod et al. 2004).

DISCUSSION

Optical properties of porewater CDOM may be influenced by both physical and biological processes, e.g. variation in quantity or composition of organic matter (OM) entering the ecosystem from production and sedimentation, photochemical and biological processing as OM is deposited, and physical soil properties. Changes in CDOM fluorescence and absorption magnitude are associated with changes in both the composition and concentration of dissolved organic compounds, while variability in spectral slope, fluorescence spectral shape and fluorescence per unit absorbance reflect changes only in CDOM composition and chemical structure (McKnight et al. 2001, Tzortziou et al. 2011). Absorption coefficients in the surface waters and porewater were generally lower in winter (wet season) vs. summer (dry season). In general, significant increases were observed in a300 below −4.5 cm depth, with decreases in bands at lower depths. Increased fluorescence relative to surface water occurred below −16.5 cm depth. Higher fluorescence and absorption are consistent with higher CDOM concentrations in porewater vs. overlying surface waters. The more intense fluorescence in porewater vs. surface waters previously observed

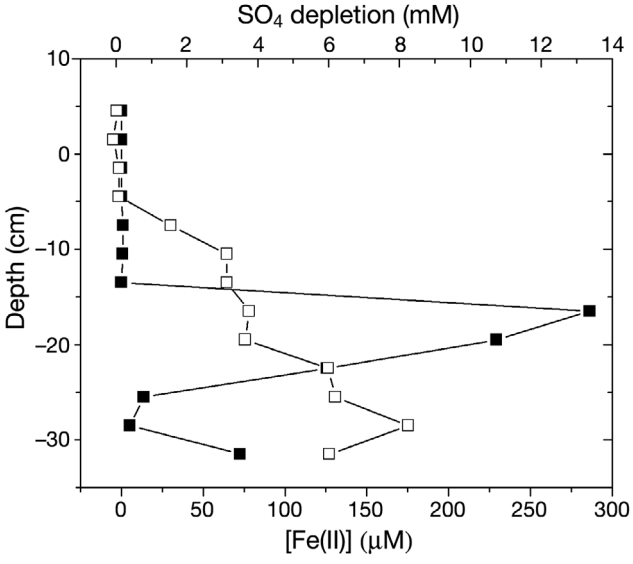

Fig. 3. Fe(II) concentration (■, µM) and SO_4 depletion (□, mM) vs. depth (cm) in porewater for site A in summer

in coastal sediments (Chen & Bada 1989) and mangroves (Marchand et al. 2006) was attributed to the release and subsequent anoxic degradation of OM released from the solid phase. Increased fluorescence with depth in suboxic sediment porewater has been directly associated with increased total dissolved organic carbon levels (Burdige et al. 2004).

We report S values here for 3 ranges to allow for intercomparison between our previous work at this site (S_1, 300 to 400 nm; Clark et al. 2008) and other marsh sediment studies (S_2, 275 to 295; S_3, 350 to 400 nm; Tzortziou et al. 2007, 2011, Helms et al. 2008); all ranges showed the same general trends. S increases as CDOM is photobleached in oxidative environments and decreases with aging in suboxic soils and sediments because of increasing aromaticity and humification (Stabenau et al. 2004, Tzortziou et al. 2007). Lower S values are indicative of CDOM that is more humic or terrestrial in nature (Green & Blough 1994, Vodacek et al. 1997). In this study, S was generally lower in the porewaters vs. surface water by as much as a factor of 10, with the most dramatic change across the soil-water interface. S values varied with depth. Burdige et al. (2004) reported S values for porewaters in estuarine sediment on the Atlantic Ocean that were only slightly lower (~20%) than the overlying waters and showed no significant variation with depth. The decrease from surface to porewater in this study would be consistent with a transition between regions where CDOM is photochemically and aerobically processed to anaerobic processing. Surface water S values in this study are on the low end of the range of 0.012 to 0.018 nm^{-1} reported for estuarine waters (Vodacek et al. 1997, Burdige et al. 2004, Stabenau et al. 2004, Tzortziou et al. 2007, Helms et al. 2008) and tidal outwelling from marshes (Tzortziou et al. 2011) but similar to values previously obtained for surface waters ebbing from this marsh (0.010 ± 0.002 nm^{-1}, Clark et al. 2008). Previous studies report S in different spectral ranges, which affects values and complicates intercomparisons (e.g. Vodacek et al. 1997 vs. Stabenau et al. 2004). S_R averaged 0.97 ± 0.15 for surface water and 1.26 ± 0.61 for porewater in winter and was similar in summer (1.00 ± 0.87 for surface water, 1.22 ± 0.82 for porewater). Average values obtained here are within the range previously obtained in the Delaware estuary (Helms et al. 2008, 0.88 to 1.32). Helms et al. (2008) attributed $S_R > 1$ in an estuarine to ocean transect to waters that are mainly marine in character vs. $S_R < 1$, which are mainly terrestrial. Since higher-MW material was associated with lower S_R values (Helms et al. 2008), the increases in S_R at depths of −7.5, −16.5 and −31.5 cm in our study suggest lower-MW material in these regions.

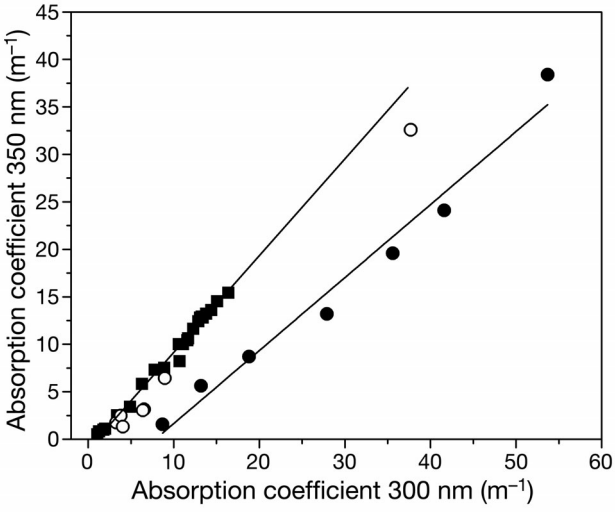

Fig. 4. Absorption coefficients (m^{-1}) at 300 nm vs. 350 nm for surface and soil porewater (m^{-1}) in winter (■) and summer (●). Lines shown from linear regression fits: (■) R^2 = 0.99, slope = 1.00 ± 0.02, intercept = −0.9 ± 0.2 (n = 23); (●) R^2 = 0.97, slope = 0.77 ± 0.06, intercept = −6.0 ± 1.7 (n = 7). Open circles (n = 7) represent a subset of the summer samples (surface and shallow porewater down to −10.5 cm and at −16.5 cm depth) which fall along the winter regression line

Oscillations in a300 and fluorescence were observed at the same depths where S_R increased. Variability in absorbance and fluorescence could be due to differences in both CDOM quantity and composition. To examine variability in composition, the ratio of absorption coefficient at 2 different values (300 and 350 nm) can be used (Clark et al. 2008); this ratio should not change for porewater with varying amounts of CDOM due to differences in deposition rate, solubility, soil conductivity or compaction. In winter, a constant ratio of 1.00 ± 0.02 across all depths suggests that CDOM in surface and porewater is from similar sources (Fig. 4; a300 vs. a350 nm; R^2 = 0.99). In summer, surface and shallower porewater samples down to −10.5 cm fall on the same line. However, deeper porewater samples are offset to the right, with lower-than-expected absorbance in the longer-wavelength region, suggesting more humified, older material. The exception is at −16.5 cm depth, which falls on the same line as for the winter samples, possibly because of OM processing and production by anaerobic bacteria.

The flu:abs ratio is one measure of CDOM composition changes, with decreasing values associated with increasing MW, humification and aromaticity (Belzile & Guo 2006). In winter, flu:abs ratios were highest in the surface waters (12 to 16) and then

decreased in the deeper porewaters to lows of 1 to 2 (Fig. 5), consistent with lower-MW material at the surface and higher-MW material at depth. The flu:abs ratio increased at depths of −7.5, −16.5 and −28.5 cm to values of 4 to 8, suggesting lower-MW material in these regions. Similar low values (1 to 2) were obtained in the deeper porewaters in summer. Increases were again observed at −7.5 and −28.5 cm, consistent with lower-MW material at these depths, possibly from enhanced microbial processing. The more intense protein peaks observed at these depths in the porewater EEMs support this hypothesis, since protein-like peaks are associated with amino acids free or bound in proteins, and the tryptophan-like peak T indicates recent origin (Yamashita & Tanoue 2003, Fellman et al. 2008). Flu:abs ratios were unusually low in the surface waters compared to winter. This could be explained by the presence of a strongly absorbing, weakly fluorescing compound in addition to the CDOM typically found in the marsh waters.

Humic-type peaks A and C were observed in all surface and porewater samples in both seasons. These have been observed in terrestrial, coastal and oceanic waters (Stedmon & Markager 2005, Clark et al. 2008). Production of humic materials from east coast Atlantic marsh plants (mangrove, sawgrass, cordgrass, sea grass) has been shown (Moran et al. 1991, Moran & Hodson 1994, Scully et al. 2004, Stabenau et al. 2004). In winter, peaks A and C in surface water may arise from autochthonous marsh-produced material and allochthonous terrestrial material from tidal inflow, runoff and rain events. The lower-intensity peaks A and C observed in surface waters in summer vs. winter are consistent with reduced DOM inputs in the summer dry season. The intensities of peaks A and C in deeper porewater in summer vs. winter were also lower, possibly because of DOM leaching from the soil reservoir depleting porewater levels.

In contrast to peaks A and C, peak M was observed only in the surface and shallow porewaters in winter. Since prior studies at this site (Clark et al. 2008) showed that several marsh plants produced peak M, this absence suggests no significant net production from marsh plants in summer. Peak M has been associated with microbial activity in seawater but also has been observed in wastewater, wetlands, salt marshes and agricultural environments (Stedmon & Markager 2005, Clark et al. 2008, Fellman et al. 2008). Peaks A, C and M have been previously observed in waters ebbing from this marsh, but only peaks A and C were routinely observed in the adjacent coastal receiving waters (Clark et al. 2008, 2009, 2010). This suggests

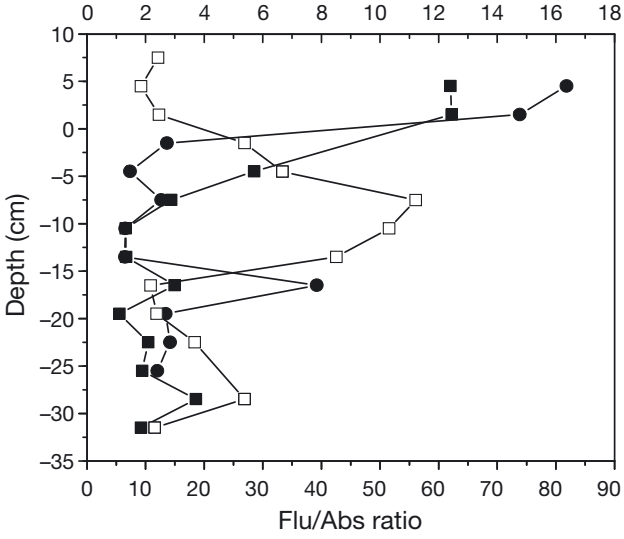

Fig. 5. Fluorescence:absorbance (flu:abs) ratio (fluorescence at $\lambda_{excitation}$ = 350 nm; $\lambda_{emission}$ = 450 nm; absorption at 300 nm) as a function of depth (cm) for site A (■) and site B (●) in winter (bottom *x*-axis) and site A (□) in summer (top *x*-axis). Lines shown for ease of viewing

that peak M is removed through the marsh-coastal water transition through photochemical or biological processing. Photodegradation of peak M from southern California salt marsh plant leachates has been previously reported, with half-lives from 10 to 20 h, on the order of the residence time of water in the marsh due to tidal flushing (Clark et al. 2008). Similarly rapid photodegradation with half-lives of 9 to 22 h was observed for fluorescing humic materials from Florida Everglades plants (Scully et al. 2004). Peak M from cordgrass has also been shown to undergo rapid oxic microbial processing into peak C (Wang et al. 2007).

Fluorescence indices provide additional evidence for potential CDOM sources. The *f*450/*f*500 index provides an estimate of the degree of aromaticity; values of ~1.9 have been obtained for aquatic and microbial sources and ~1.3 for terrestrial and soil sources (McKnight et al. 2001). Values of 1.2 to 1.3 for surface water and porewater samples in winter and porewater samples in summer are consistent with predominantly terrestrial and soil sources, whereas a higher value of 1.8 for surface waters in summer suggests aquatic and microbial sources. The HIX index is another measure of aromaticity and the degree of maturation (Zsolnay et al. 1999). Higher values (10 to 16) are associated with highly humified OM of predominately terrestrial origin, whereas lower values (<4) have been associated with autochthonous OM (Huguet et al. 2010). In this study, HIX values ranged

from highs of 7 to 10 in the winter to lows of 2 to 4 in the summer. In both seasons, HIX values were higher in the porewater vs. surface water, consistent with increased humification in soil. Decreases in HIX values at depths of −7.5, −16.5 and −28.5 cm suggested the presence of autochthonous OM in these regions, possibly from enhanced microbial processing. The more intense protein peaks observed at these depths in the porewater EEMs support this hypothesis, since protein-like peaks are associated with amino acids free or bound in proteins, and the tryptophan-like peak T indicates recent origin (Yamashita & Tanoue 2003, Fellman et al. 2008). The BIX index is a measure of autochthonous biological activity in estuarine and marine environments; higher values (>1) are attributed to autochthonous DOM and OM freshly released in water, whereas lower values (0.6 to 0.7) are associated with reduced *in situ* DOM production (Huguet et al. 2010). BIX values of 0.7 obtained for the surface and most porewaters in this study in winter and summer are consistent with a predominately allochthonous terrestrial DOM source. Some higher values, for example 0.9 at −7.5 cm depth in summer, indicate that increased *in situ* production may occur in some regions.

These results overall suggest that DOM in porewater arises primarily from imported allochthonous terrestrial humic material in addition to autochthonous microbial and aquatic sources. Another DOM source that could be significant is importation of marine particles on the incoming tide, which may deposit in the marsh, solubilize to DOM and be exported on outgoing tides. Prior studies have shown high levels of pheophytin in marine sediments in the Pacific Ocean due to diagenesis and deposition of plankton-derived marine particles (Wakeham et al. 1997, Lee et al. 2000). The intense peak we observed in deeper porewater in winter with optical characteristics consistent with chlorophyll or its degradation product pheophytin (French et al. 1956, Krauss & Weiss 1991, Hense et al. 2008) would be consistent with deposition of marine particles. The lower levels in the summer study may arise from seasonal variations in phytoplankton production.

CONCLUSIONS

Results from this study suggest that soil porewater is a major reservoir of CDOM in the salt marsh, with organic material from terrestrial watershed inputs and *in situ* production from marsh vegetation stored and processed in sediments. Optical property trends from surface waters to porewater are attributed to differences in biological and photochemical processing in oxic and anoxic environments. At the transition from surface water into deeper soil porewater, increased absorption and fluorescence correlated with red-shifted emission wavelengths, and lower flu:abs ratios suggest more aromatic, higher-MW material. Bands at depths of −16.5 and −28.5 cm, where absorption decreases, fluorescence increases, flu:abs ratio increases and HIX decreases, are associated with tryptophan-type protein T peaks, blue-shifted emission wavelengths for peak A and variations in Fe(II) concentrations and SO_4 depletion. We hypothesize that these optical property changes at anoxic depths are due to enhanced anaerobic microbial activity producing remineralized, lower-MW DOM, with the dominant metabolism pathway potentially varying from sulfate to iron reduction.

Acknowledgements. C.D.C., W.J.D. and J.K.K. thank the National Science Foundation for support (C.D.C. and W.J.D., Division of Ocean Sciences grant #072528433; J.K.K., Division of Environmental Biology grant #0816743); students Benjamin Brahm, Moises Ahrani, Jenny Bowen and Brenna McNabb for assistance with sampling and peeper preparation; Kimberly Takagi for ion chromatography; and Erin Hardison, US Army Corps of Engineers, for site information and access.

LITERATURE CITED

Belzile C, Guo L (2006) Optical properties of low molecular weight and colloidal organic matter: application of the ultrafiltration permeation model to DOM absorption and fluorescence. Mar Chem 98:183–196

Berner RA (1964) Distribution and diagenesis of sulfur in some sediments from the Gulf of California. Mar Geol 1: 117–140

Bianchi TS (2007) Biogeochemistry of estuaries. Oxford University Press, Oxford

Boyd TJ, Osburn CL (2004) Changes in CDOM fluorescence from allochthonous and autochthonous sources during tidal mixing and bacterial degradation in two coastal estuaries. Mar Chem 89:189–210

Burdige DJ, Kline SW, Chen W (2004) Fluorescent dissolved organic matter in marine sediment porewaters. Mar Chem 89:289–311

Chen RF, Bada JL (1989) Seawater and porewater fluorescence in the Santa Barbara Basin. Geophys Res Lett 16: 687–690

Chen RF, Gardner GB (2004) High-resolution measurements of chromophoric dissolved organic matter in the Mississippi and Atchafalaya River plumes. Mar Chem 89: 103–125

Chmura GL, Ansfield SC, Cahoon DR, Lynch TC (2003) Global carbon sequestration in tidal, saline wetland soils. Global Biogeochem Cycles 17:1111, doi:10.1029/2002GB001917

Clark CD, Litz LP, Grant SB (2008) Saltmarshes as a source of

chromophoric dissolved organic matter to southern California coastal waters. Limnol Oceanogr 53:1923–1933

Clark CD, De Bruyn WJ, Jones JG (2009) Photochemical production of hydrogen peroxide in size-fractionated southern California coastal waters. Chemosphere 76: 141–146

Clark CD, De Bruyn WJ, Hirsch CB, Jakubowski SD (2010) Spatial and temporal measurements of hydrogen peroxide concentrations in recreational marine bathing waters in southern California. Water Res 44:2203–2210

Coble PG (1996) Characterization of marine and terrestrial DOM in seawater using excitation-emission matrix spectroscopy. Mar Chem 51:325–346

de Souza Sierra MM, Donard OFX, Lamotte M (1997) Spectra identification and behavior of dissolved organic fluorescent material during estuarine mixing processes. Mar Chem 58:51–58

Elrod VA, Berelson WM, Cole KH, Johnson KS (2004) The flux of iron from continental shelf sediments: a missing source for global budgets. Geophys Res Lett 31:L12307, doi:10.1029/2004GL020216

Fellman JB, D'Amore DV, Hood E, Boone RD (2008) Fluorescence characteristics and biodegradability of dissolved organic matter in forest and wetland soils from coastal temperate watersheds in southeast Alaska. Biogeochemistry 88:169–184

French CS, Smith JHC, Virgin HI, Airth R (1956) Fluorescence-spectrum curves of chlorophylls, pheophytins, phycoerythrins, phycocyanins and hypericin. Plant Phys 31:369–374

Gallegos CL, Jordan TE, Hines AH, Weller DE (2005) Temporal variability of optical properties in a shallow, eutrophic estuary: seasonal and interannual variability. Estuar Coast Shelf Sci 64:156–170

Gardner GB, Chen RF, Berry A (2005) High-resolution measurements of chromophoric dissolved organic matter (CDOM) in the Neponset River estuary, Boston Harbor, MA. Mar Chem 96:137–154

Green S, Blough NV (1994) Optical absorption and fluorescence properties of chromophoric dissolved organic matter in natural waters. Limnol Oceanogr 39:1903–1916

Helms JR, Stubbins A, Ritchie JD, Minor EC, Kieber DJ, Mopper K (2008) Absorption spectral slopes and slope ratios as indicators of molecular weight, source, and photobleaching of chromophoric dissolved organic matter. Limnol Oceanogr 53:955–969

Hense BA, Gais P, Jutting U, Scherb H, Rodenacker K (2008) Use of fluorescence information for automated phytoplankton investigation by image analysis. J Plankton Res 30:587–606

Hesslein RH (1976) An *in situ* sampler for close interval porewater studies. Limnol Oceanogr 21:912–914

Hu C, Muller-Karger FE, Zepp RG (2002) Absorbance, a(300) and apparent quantum yield: a comment on common ambiguity in the use of these optical concepts. Limnol Oceanogr 47:1261–1267

Huguet A, Vacher L, Saubusse S, Etcheber H and others (2010) New insights into the size distribution of fluorescent dissolved organic matter in estuarine waters. Org Geochem 41:595–610

Keller JK, Wolf AA, Weisenhorn PB, Drake BG, Megonigal JP (2009) Elevated CO_2 affects porewater chemistry in a brackish marsh. Biogeochemistry 96:101–117

Krause GH, Weis E (1991) Chlorophyll fluorescence and photosynthesis: the basics. Annu Rev Plant Physiol Plant Mol Biol 42:313–349

Lee C, Wakeham SG, Hedges JI (2000) Composition and flux of particulate amino acids and chloropigments in equatorial Pacific seawater and sediments. Deep-Sea Res 47:1535–1568

Leslie BW, Hammond DE, Berelson W, Lund SP (1990) Diagenesis in anoxic sediments from the California continental borderland and its influence on iron, sulfur, and magnetite behavior. J Geophys Res 95:4453–4470

Lovley DR, Phillips EJP (1986) Organic matter mineralization with reduction of ferric iron in anaerobic sediments. Appl Environ Microbiol 51:683–689

Marchand C, Albéric P, Lallier-Vergès EF (2006) Distribution and characteristics of dissolved organic matter in mangrove sediment porewaters along the coastline of French Guiana. Biogeochemistry 81:59–75

McKnight DM, Boyer EW, Westerhoff PK, Doran PT, Kulbe T, Andersen DT (2001) Spectrofluorometric characterization of dissolved organic matter for indication of precursor organic material and aromaticity. Limnol Oceanogr 46:38–48

Mclusky DS, Elliot M (2004) The estuarine ecosystem: ecology, threats and management, 3rd edn. Oxford University Press, Oxford

Megonigal JP, Hines ME, Visscher PT (2004) Anaerobic metabolism: linkages to trace gases and aerobic processes. In: Schlesinger WH (ed) Biogeochemistry. Elsevier Pergamon, Oxford, p 317–424

Miller WL (1998) Effects of UV radiation on aquatic humus: photochemical principles and experimental considerations. In: Hessen DO, Tranvik LJ (eds) Aquatic humic substances: ecology and biogeochemistry. Springer-Verlag, Berlin, p 125–143

Mopper K, Schultz K (1993) Fluorescence as a possible tool for studying the nature and water column distribution of DOC components. Mar Chem 41:229–235

Moran MA, Hodson RE (1989) Formation and bacterial utilization of dissolved organic carbon derived from detrital lignocellulose. Limnol Oceanogr 34:1034–1037

Moran MA, Hodson RE (1994) Dissolved humic substances of vascular plant origin in a coastal marine environment. Limnol Oceanogr 39:762–771

Moran MA, Zepp RG (1997) Role of photoreactions in the formation of biologically labile compounds from dissolved organic matter. Limnol Oceanogr 42:1307–1316

Moran MA, Wicks RJ, Hodson RE (1991) Export of dissolved organic matter from a mangrove swamp ecosystem: evidence from natural fluorescence, dissolved lignin phenols, and bacterial secondary production. Mar Ecol Prog Ser 76:175–184

Moran MA, Sheldon WM, Zepp RG (2000) Carbon loss and optical property changes during long-term photochemical and biological degradation of estuarine dissolved organic matter. Limnol Oceanogr 45:1254–1264

Murphy KR, Stedmon CA, Waite TD, Ruiz GM (2008) Distinguishing between terrestrial and autochthonous organic matter sources in marine environments using fluorescence spectroscopy. Mar Chem 108:40–58

Otero M, Mendonça A, Válega M, Santos EBH, Pereira E, Esteves VI, Duarte A (2007) Fluorescence and DOC contents of estuarine porewaters from colonized and non-colonized sediments: effects of sampling preservation. Chemosphere 67:211–220

Rochelle-Newall EJ, Fisher TR (2002) Chromophoric dissolved organic matter and dissolved organic carbon in

Chesapeake Bay. Mar Chem 77:23–41

Scully NM, Maie N, Dailey SK, Boyer JN, Jones RD, Jaffe R (2004) Early diagenesis of plant-derived dissolved organic matter along a wetland, mangrove, estuary ecotone. Limnol Oceanogr 49:1667–1678

Stabenau ER, Zepp RG, Bartels E, Zika RG (2004) Role of the seagrass *Thalassia testudinum* as a source of chromophoric dissolved organic matter in coastal south Florida. Mar Ecol Prog Ser 282:59–72

Stedmon CA, Markager S (2005) Resolving the variability in dissolved organic matter fluorescence in a temperate estuary and its catchment using PARAFAC analysis. Limnol Oceanogr 50:686–697

Stedmon CA, Markager S, Bro R (2003) Tracing dissolved organic matter in aquatic environments using a new approach to fluorescence spectroscopy. Mar Chem 82: 239–254

Tobias C, Neubauer SC (2009) Salt marsh biogeochemistry—an overview. In: Perillo GME, Wolanski E, Cahoon DR, Brinson MM (eds) Coastal wetlands: an integrated ecosystem approach. Elsevier, Amsterdam, p 445–492

Tzortziou M, Osburn CL, Neale PJ (2007) Photobleaching of dissolved organic material from a tidal marsh-estuarine system of the Chesapeake Bay. Photochem Photobiol 83: 782–792

Tzortziou M, Neale PJ, Megonigal JP, Pow CL, Butterworth M (2011) Spatial gradients in dissolved organic carbon due to tidal marsh outwelling into a Chesapeake Bay estuary. Mar Ecol Prog Ser 426:41–56

Vahatalo AV, Wetzel RG (2008) Long-term photochemical and microbial decomposition of wetland-derived dissolved organic matter with alteration of ^{13}C:^{12}C mass ratio. Limnol Oceanogr 53:1387–1392

Vodacek A, Blough NV, DeGrandpre MD, Peltzer ET, Nelson RK (1997) Seasonal variation of CDOM and DOC in the Middle Atlantic Bight: terrestrial inputs and photooxidation. Limnol Oceanogr 42:674–686

Wakeham SG, Lee C, Hedges JI, Hernes PJ, Peterson ML (1997) Molecular indicators of diagenetic status in marine organic matter. Geochim Cosmochim Acta 61: 5363–5369

Wang XC, Litz L, Chen RF, Huang W, Feng P, Altabet MA (2007) Release of dissolved organic matter during oxic and anoxic decomposition of salt marsh cordgrass. Mar Chem 105:309–321

Yamashita Y, Tanoue E (2003) Chemical characterization of protein-like fluorophores in DOM in relation to aromatic amino acids. Mar Chem 82:255–271

Zsolnay A, Baigar E, Jiminez M, Steinweg B, Saccomandi F (1999) Differentiating with fluorescence spectroscopy the sources of dissolved organic matter in soils subjected to drying. Chemosphere 38:45–50

Editorial responsibility: Toshi Nagata, Kashiwanoha, Japan

Submitted: July 26, 2013; Accepted: April 4, 2014
Proofs received from author(s): November 20, 2014